Supplementary Information

The Role of Bi-Polar Plate Design and the Start-up Protocol in the Spatiotemporal Dynamics during Solid Oxide Fuel Cell Anode Reduction

Thomas M. M. Heenan [1,2,*], Seyed Ali Nabavi [3], Maria Erans [3,4], James B. Robinson [1,2], Matthew D. R. Kok [1,2], Maximilian Maier [1], Daniel J. L. Brett [1,2], Paul R. Shearing [1,2] and Vasilije Manovic [3,*]

[1] Electrochemical Innovation Lab, Department of Chemical Engineering, University College London, London WC1E 7JE, UK; j.b.robinson@ucl.ac.uk (J.B.R.); m.kok@ucl.ac.uk (M.D.R.K.); maximilian.maier.17@ucl.ac.uk (M.M.); d.brett@ucl.ac.uk (D.J.L.B.); p.shearing@ucl.ac.uk (P.R.S.)
[2] The Faraday Institution, Quad One, Harwell Science and Innovation Campus, Didcot, OX11 0RA, UK
[3] Centre for Climate and Environmental Protection, Cranfield University, Bedford, MK43 0AL, UK; s.nabavi@cranfield.ac.uk (S.A.N.); Maria.Eransmoreno@nottingham.ac.uk (M.E.)
[4] Faculty of Engineering, University of Nottingham, Nottingham, NG7 2RD, UK
* Correspondence: t.heenan@ucl.ac.uk (T.H); v.manovic@cranfield.ac.uk (V.M)

Table S1. Technical information as provided by the supplier.

Specification	Details
Product type	Anode-supported cell
Cathode material	LSCF [1] + GDC [2]
Cathode thickness /μm	20–25
Diffusion Barrier Layer Material	GDC
Diffusion Barrier Layer thickness /μm	2–3
Electrolyte material	YSZ [3]
Electrolyte thickness /μm	10–15
Anode material (as supplied)	NiO [4] + YSZ
Anode thickness /μm	400
Interconnects	SUS430
Bending strength /MPa	≥250
Power density [5] /W cm^{-2}	≥0.7
Square cell size /cm × cm	15 × 15

[1] LSCF—lanthanum strontium cobalt ferrite; [2] GDC—gadolinium-doped ceria; [3] YSZ—yttria-stabilized zirconia; [4] NiO—nickel oxide tables may have a footer; [5] at 750 °C and 0.7 V.

More information can be found on the manufacturer's webpage: http://www.sofcman.com/default.asp.

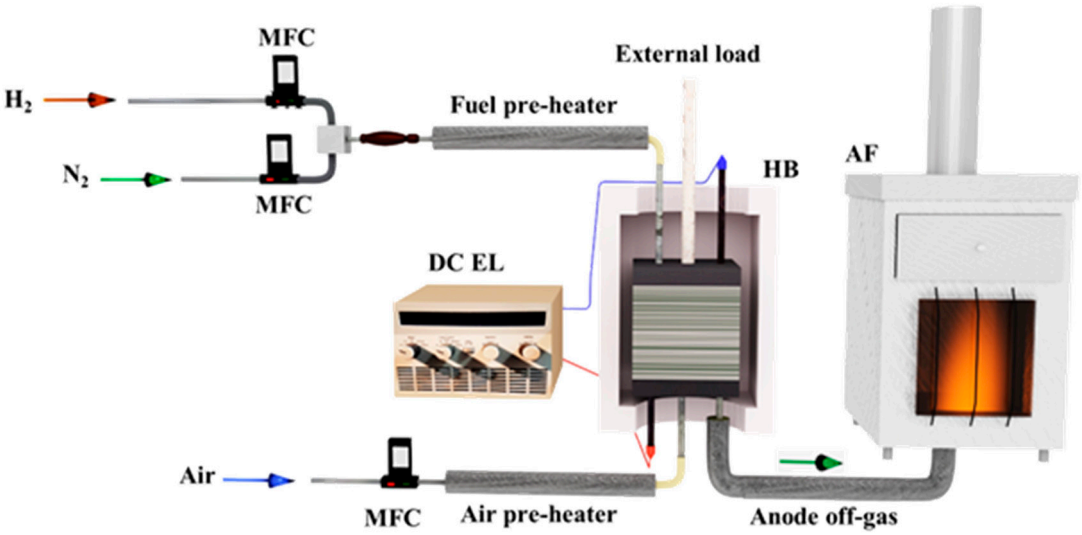

Figure S1. Schematic diagram of the experimental setup for the operation of a 2 $kW_{el,DC}$ Figure 30. Planar 14 × 14 cm anode-supported cells and a configuration of Ni–YSZ/YSZ/CGO/LSCF-CGO, operating on pre-heated hydrogen and air feeds.

Table S2. Variation of average cell voltage and stack temperature during the reduction of the 30 cell SOFC stack.

Time /min	Flow rates /L min^{-1}		Average Cell OCV /Volts	Stack Temperature /°C
	Hydrogen	Air		
0	4	12	0.55	750
10	4	12	0.53	768
59	4	12	0.53	768
60	4	28	0.72	783
90	4	28	0.71	783
105	4	28	0.71	783
125	4	28	0.70	783
142	4	28	0.71	783
156	4	28	0.71	783
170	4	28	0.70	783
185	4	28	0.70	783
195	14	70	0.81	783
205	14	79	0.76	783

The stack reduction was initiated by the introduction of 4 L min^{-1} hydrogen and 12 L min^{-1} air, resulting in an initial open circuit voltage (OCV) of 0.55 V (averaged per cell), which eventually dropped to 0.53 V, and remained relatively constant for the subsequent 1 h. In addition, there was a sudden increase in furnace temperature from 750 to 768 °C, once hydrogen was fed into the stack. The manufacturer's recommendations state that the anode reduction is completed when a stable stack OCV of ~34.2 V is achieved (1.14 V per cell). Since no rise in OCV was observed after 1 h, the air flow-rate was increased to 28 L min^{-1}, which led to an OCV of 0.72 V, and the furnace temperature of 783 °C. After 2 h, there was only a negligible variation in OCV from 0.72 to 0.70 V. Therefore, the hydrogen and air flow-rates were gradually increased to 14 L min^{-1} and 70 L min^{-1} respectively, which resulted in an OCV of 0.81 V. Furthermore, the air flow rate was increased to 79 L min^{-1} which caused a reduction in OCV to 0.76 V. The variation of OCV and stack temperature during the reduction is tabulated in Table S1.

Table S3. Polarization data from the 30 cell SOFC stack at ca. 783 °C.

Hydrogen Flowrate /L min^{-1}	Air Flowrate /L min^{-1}	Stack Current /Amps	Stack Potential /Volts	Average Cell Potential /Volts	Stack Power /Watts
14	70	0.00	24.22	0.81	0.00
14	79	0.00	22.80	0.76	0.00
14	79	0.10	17.20	0.57	1.72
14	79	0.20	14.70	0.49	2.94
14	79	0.30	12.50	0.42	3.75
14	79	0.40	10.60	0.35	4.24
14	79	0.50	8.40	0.28	4.20
14	79	0.60	7.30	0.24	4.38
14	79	0.70	5.10	0.17	3.57
14	79	0.80	3.00	0.10	2.40
14	79	0.90	0.70	0.02	0.63
14	79	0.80	3.00	0.10	2.40
14	79	0.70	5.20	0.17	3.64
14	79	0.60	7.20	0.24	4.32
14	79	0.50	9.40	0.31	4.70
14	79	0.40	11.20	0.37	4.48
14	79	0.30	13.00	0.43	3.90
14	79	0.20	15.20	0.51	3.04
14	79	0.10	17.20	0.57	1.72
14	79	0.00	21.40	0.71	0.00
19	80	0.00	13.10	0.44	0.00

During the operation/polarization step, the stack current was gradually increased from 0.0 to 0.9 A, which resulted in a significant reduction in cell potential from 0.76 to 0.02 V, indicating poor performance of the stack. The cell potential during operation, i.e., while pulling a current, gives an indication of the performance of the stack by the difference between the operating potential and the open circuit potential; the larger the difference the greater the overpotential losses and poorer performance. Overpotential losses can always be expected in a real-world system due to entropy; however, they should be minimized in order to operate as efficiently as possible. The stack current was then gradually reduced back to 0.0 A, for which an OCP of 0.71 V was achieved; polarization and power curves can be seen in Figure S2a and S2b. Further increases in the hydrogen and air flow rates to 19 L min^{-1} and 80 L min^{-1} led to a sudden drop in OCP to 0.44 V, and elevation of the furnace temperature to 840 °C. The temperature rise along with a simultaneous sudden drop in OCP, while both hydrogen and air flow rates increased, indicated the possibility of gas leakage from the cells, and subsequent failure of the stack, at was further proven in the leakage test, Figure S3. The electrochemical performance of this stack is substantially lower than what would be expected from a stack of this size. Therefore, some part of the operational start-up was clearly ineffective.

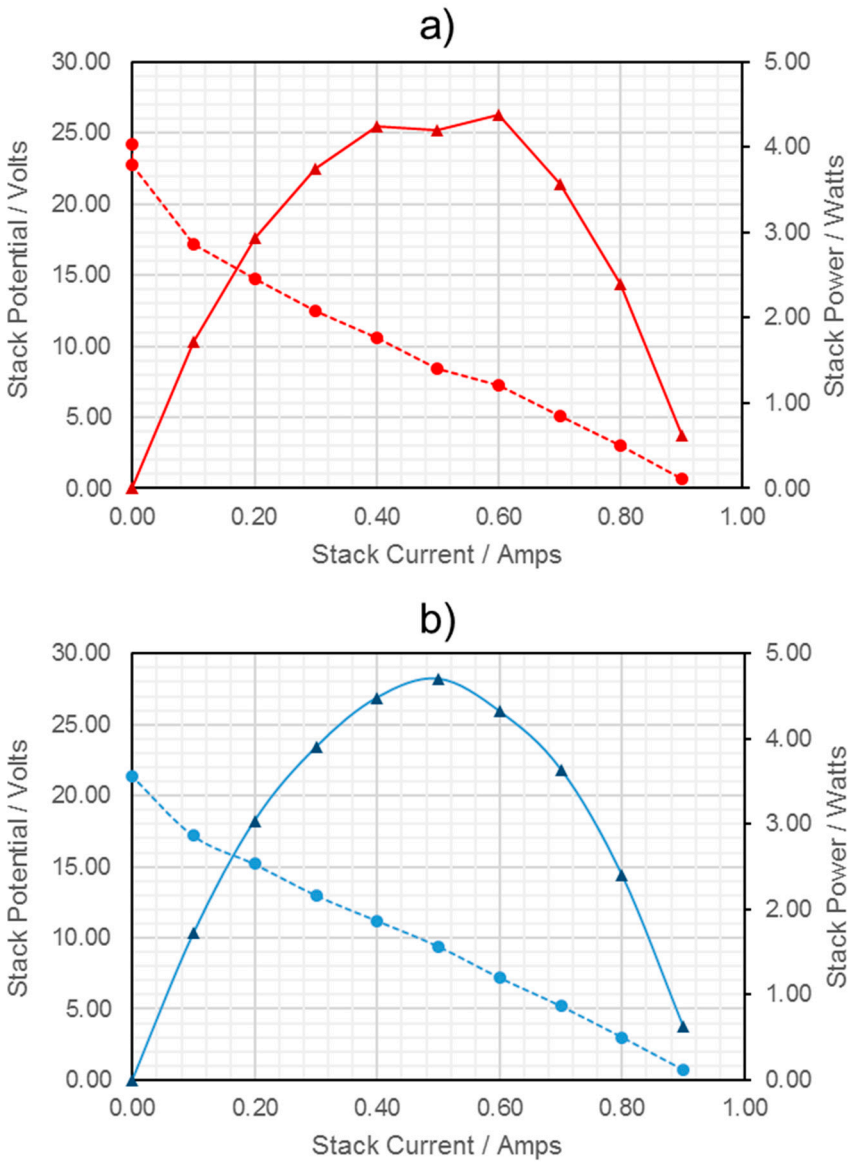

Figure S2. Electrochemical data extracted from the SOFC stack: polarization curves collected at 783 °C with flowrates of 14 and 79 L min^{-1} of hydrogen and air on the anodes and cathodes, respectively, during (**a**) increasing and (**b**) decreasing current, and (**c**) the stack potentials for the post-reduction cycle (after ca. 4 hour reduction under H_2), pre-operation, post-operation and after a cell or cells failed due to a leak.

Visually comparing the stack before and after the test, it could be seen that there was a burned zone on the front and cathode off-gas exit of the stack, which could have been caused by a large localized leak of hydrogen into the exhaust air, and consequent combustion, Figure S1. The possibility of anode leaking into the exhaust air was tested by the introduction of 2–4 L min^{-1} nitrogen into the anode side of the stack and using a liquid leak detector at the cathode exit. The formation of bubbles on the cathode exit confirmed the leak.

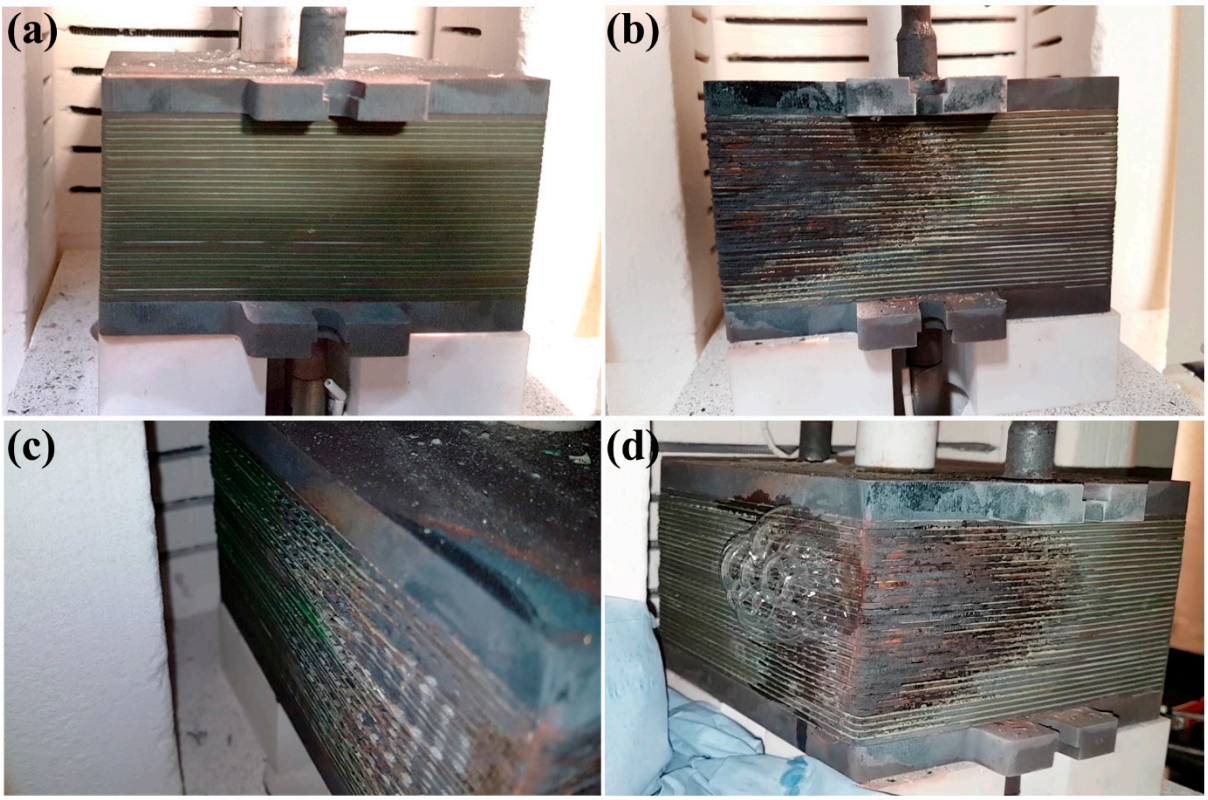

Figure S3. SOFC stack (**a**) prior to the test; (**b** and **c**) after the test; (**d**) during the leak detection test.

Table S4. Various NiO [1] and YSZ [2] peak locations. [37–39]

Material	Definition	Raman Shift /cm^{-1}
NiO	2M	1490
NiO	2P (2LO)	1090
NiO	2P (TO + LO)	906
NiO	2P (2TO)	730
YSZ	Tetragonal	643
YSZ	Tetragonal	606
NiO	1P (TO/LO)	570
YSZ	Monoclinic	480
YSZ	Tetragonal	461
YSZ	Tetragonal	319
YSZ	Tetragonal	264

[1] Lughi et al. & Clarke et al; [2] Mironova-Ulmane et al.

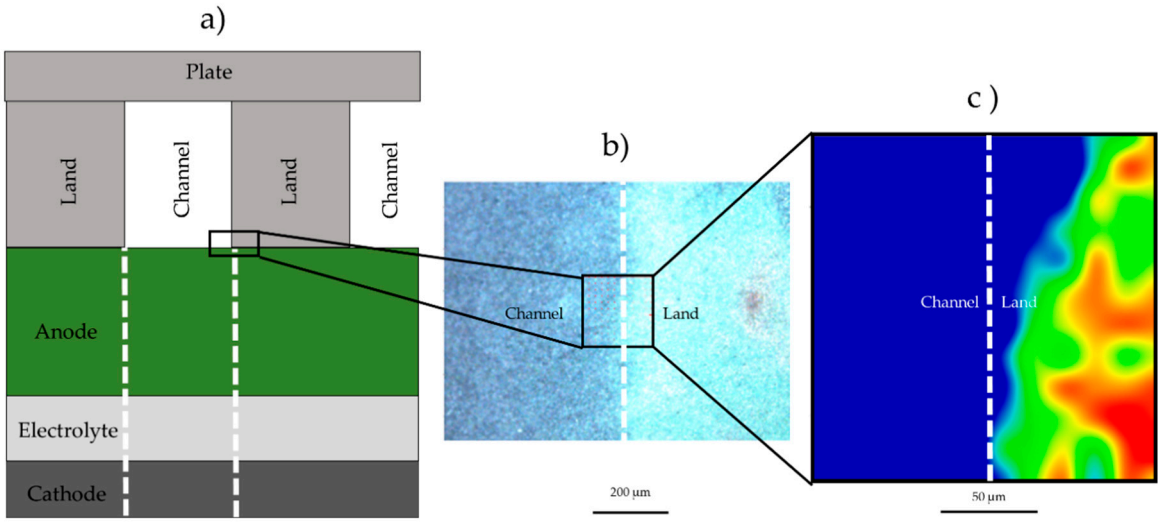

Figure S4. Correlating the positioning of the **a**) BPP, **b**) green/grey interface and **c**) Raman-active interface.

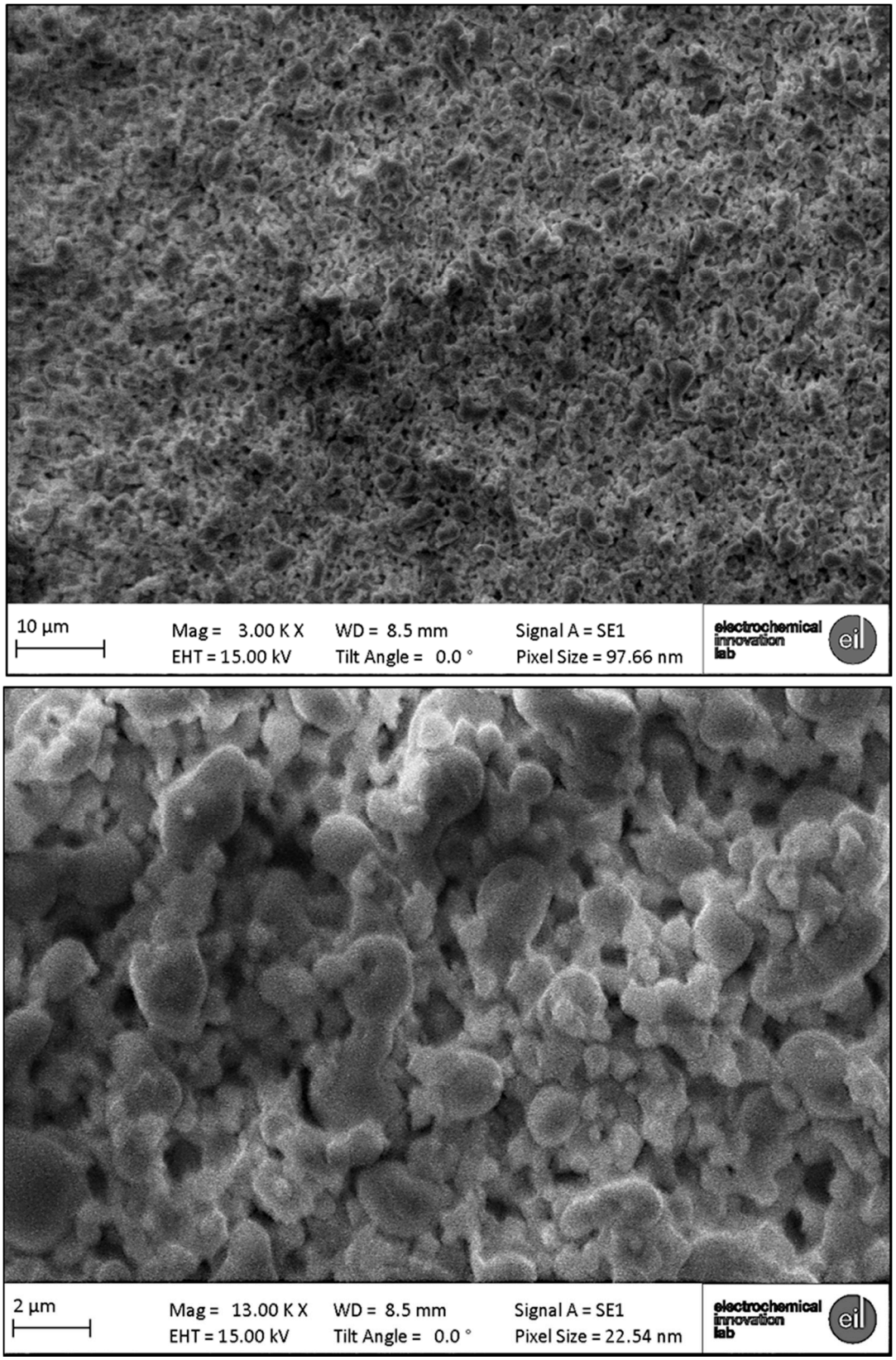

Figure S5. SEM images under the channel where the material is predominantly reduced Ni.

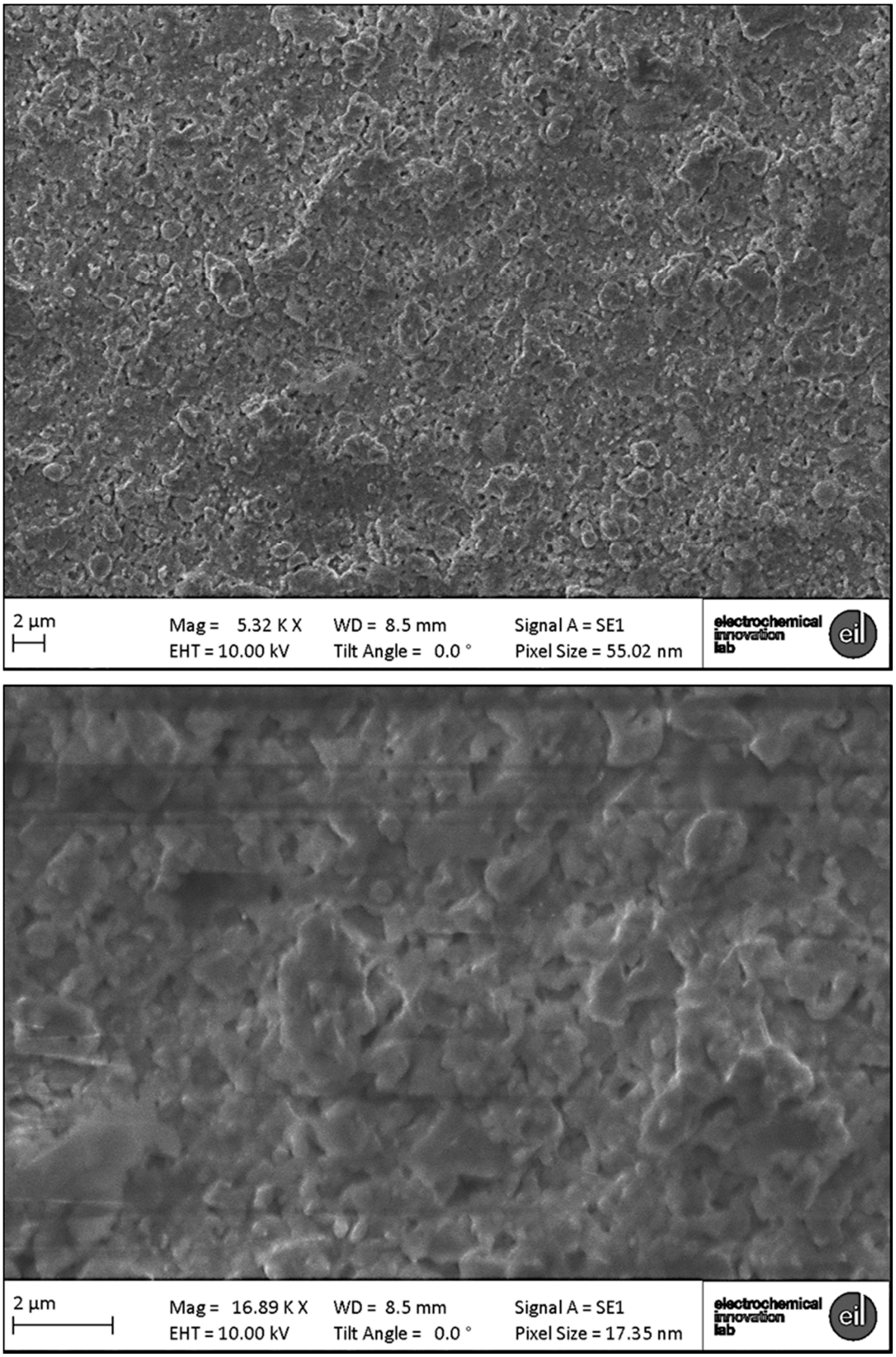

Figure S6. SEM images under the land where the material is predominantly reduced NiO.

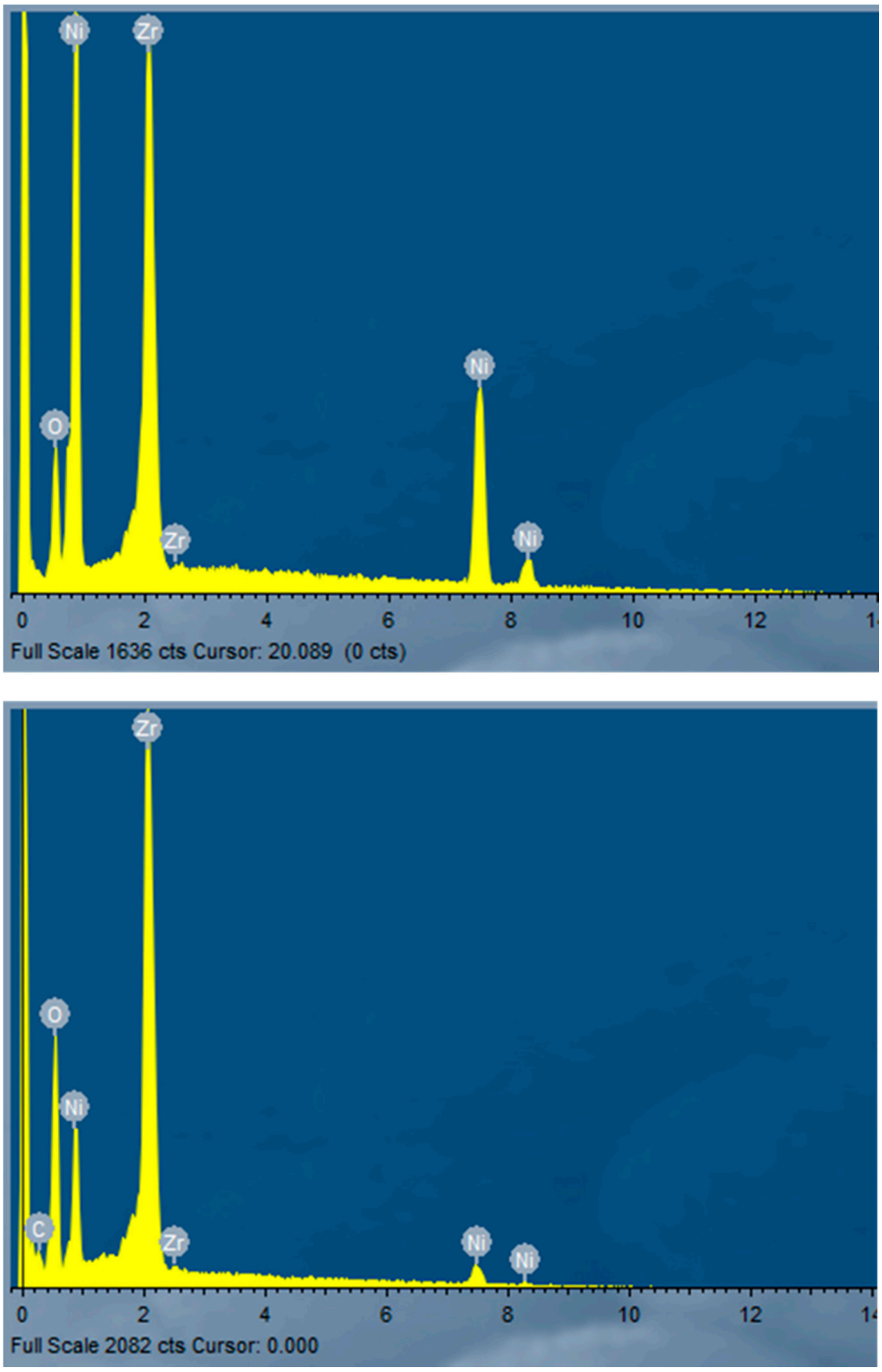

Figure S7. EDX profiles to accompany the SEM images in Figures S5 (top) and S6 (bottom).